

On the Dome Effect of Eppley Pyrgeometers and Pyranometers

Qiang Ji

SSAI, NASA Goddard Space Flight Center, Greenbelt, Maryland

Si-Chee Tsay

Laboratory for Atmospheric Sciences, NASA/GSFC, Greenbelt, Maryland

Abstract. Pyrgeometers and Pyranometers are fundamental instruments widely used for quantifying atmosphere-surface energetics in climate studies. The dome effect of these instruments can cause a measurement uncertainty larger than 10 W m^{-2} . Based on careful analysis, the dome factors of our two new pyrgeometers are found to lie in the range between 1.1 and 2.0. These values are far smaller than the value of 4.0 suggested by the World Meteorological Organization. The laboratory-determined dome factors fall within this range, if pyrgeometers approach equilibrium with the blackbody target during calibration cycles. From recent field campaigns, consistent results for the dome factors are also obtained by analyzing nighttime pyrgeometer measurements, which were regarded as approaching equilibrium state. Furthermore, we utilized an energy balance equation to describe the thermal dome effect of pyranometers that is commonly referred to as the nighttime negative outputs or the dark-offset. Lacking direct measurements of the dome and case temperatures of pyranometer, we used measurements from a pyrgeometer to derive and to account for the thermal dome effect of collocated pyranometers. This approximation revealed a reasonable agreement between calculations and measurements.

1. Introduction

Eppley Precision Infrared Radiometers (Pyrgeometer, model PIR) and Precision Spectral Pyranometers (model PSP) are widely used for measuring terrestrial (i.e., 4 to $50 \mu\text{m}$) and solar (i.e., 0.28 to $2.8 \mu\text{m}$) irradiance, respectively. PIR and PSP use the same case and sensor (thermopile) but different types of dome. A dome acts as both protection and a filter to the sensor. It also isolates the thermopile from convection. However, a dome alters the radiation balance between the sensor and the target, and introduces the dome effect.

For PIRs, the dome effect is roughly characterized in the energy balance equation by a “dome factor,” D , which is the longwave emission divided by the longwave transmission of a PIR dome, although the thermopile sensitivity is also a function of dome properties. In the World Meteorological Organization literature [Olivieri, 1991], $D \cong 4.0$. However,

it is not trivial to determine the dome factor [e.g., Philipona *et al.*, 1995]. We found that one may infer a larger value of the dome factor if the PIR does not reach equilibrium with the target during calibration. The non-equilibrium effect can also be seen by comparing daytime and nighttime field measurements.

Lacking precise theoretical analysis, the thermal dome effect of a PSP, which can cause an underestimation of the downwelling irradiance exceeding 10 W m^{-2} [Bush *et al.*, 2000], has been ignored or crudely corrected for decades. In order to use the PSP to determine the role of clear sky solar radiative fluxes [e.g., Valero and Bush, 1999], aerosol direct radiative forcing [e.g., Charlson and Heintzenberg, 1995], and the cloud absorption anomaly [e.g., Stephens and Tsay, 1990; Pilewskie and Valero, 1995] in climate studies, the dome effect must be considered. To support the experimental results by Bush *et al.* [2000], we provide a theoretical explanation of the thermal dome effect of the PSP. In addition, the nighttime negative outputs of a PSP (dark-offset) in field experiments are demonstrated to be the result of thermal dome effect.

2. Energy Balance

Fairall *et al.* [1998] reviewed relevant issues associated with the calibration of longwave radiometers. We follow their equations and add a shortwave term. Figure 1 illustrates the energy balances in a broadband radiometer. We do not consider the spectral response, and assume that the system reaches equilibrium. L and S are respectively the ambient longwave and shortwave irradiances (W m^{-2}). R_{up} and R_{down} are the total upward and downward irradiances underneath the dome. T_d , T_s , and T_c are respectively the temperature (K) of the dome, the sensor surface, and the case.

The energy balance [cf. Fairall *et al.*, 1998] of a PIR or PSP system is described by:

$$R_{\text{down}} - R_{\text{up}} = k\alpha\Delta V \quad (1a)$$

$$\epsilon_s\sigma T_s^4 + \rho_s R_{\text{down}} = R_{\text{up}} \quad (1b)$$

$$S\tau_{\text{sw}} + L\tau + \epsilon_d\sigma T_d^4 + \rho_d R_{\text{up}} = R_{\text{down}} \quad (1c)$$

$$\epsilon_s + \rho_s = 1 \quad (1d)$$

$$\tau + \epsilon_d + \rho_d = 1 \quad (1e)$$

$$T_c + \alpha\Delta V = T_s. \quad (1f)$$

Here k ($\text{W m}^{-2} \text{K}^{-1}$) is the thermal conductivity of the thermopile; $\alpha = 694 \text{ K V}^{-1}$ [cf. Payne and Anderson, 1999]; $\sigma = 5.6697 \times 10^{-8} \text{ W m}^{-2} \text{K}^{-4}$ is the Stefan-Boltzmann constant; ΔV is the output voltage of the thermopile. τ , ϵ , and

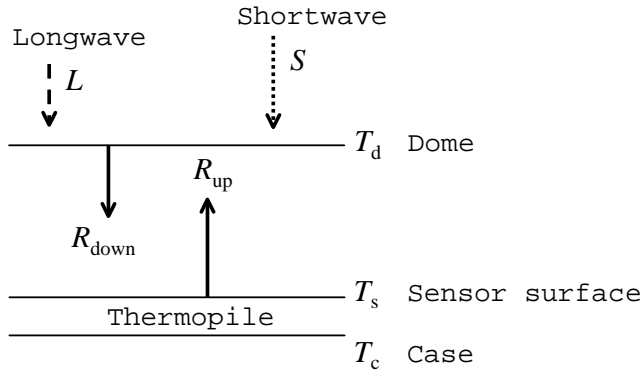


Figure 1. Schematic diagram of energy balance for PIR or PSP. L is the longwave irradiance from a target; S is the shortwave irradiance; R_{down} and R_{up} are the downward and the upward irradiances between the dome and the thermopile. T_c , T_d , and T_s are the temperature of the case, the dome, and at the upper surface of the thermopile, respectively.

ρ (dimensionless) denote respectively the longwave transmittance, emittance, and reflectance, with subscript “d” for dome and “s” for sensor; τ_{sw} (dimensionless) is the shortwave transmittance of the dome. For the PIR, the dome reflects and absorbs almost all the shortwave radiation, therefore, $\tau_{\text{sw}} \approx 0$ (no “shortwave leak”). For the PSP, on the other hand, $\tau_{\text{sw}} \approx 1$. The characteristics of the dome transmittance, together with the normalized Planck functions at 5700 K and 300 K are shown in Fig. 2.

3. PIR Dome Factor

By solving Eq. (1) for longwave irradiance L ($\tau_{\text{sw}} \approx 0$) as a function of the directly measured quantities T_d , T_c , and ΔV , one finds:

$$L = \left[\frac{1}{s_0} + 4\alpha(1+D)\sigma T_c^3 \right] \Delta V + \sigma T_c^4 + D\sigma(T_c^4 - T_d^4) + O(\Delta V^2) \quad (2a)$$

$$\frac{1}{s_0} = k[1 - (1 - \epsilon_s)\rho_d]\alpha \frac{1}{\epsilon_s T} \quad (2b)$$

$$D = \frac{\epsilon_d}{\tau} \quad (2c)$$

where s_0 is a sensitivity constant that depends on the physical characteristics of the sensor and the dome, and D is the dome factor. T_d is measured by a thermistor mounted on the dome, assuming uniformity of temperature field across the dome. From Eq. (2a), by letting $4\alpha\sigma T_c^3 \Delta V + \sigma(T_c^4 - T_d^4) = 0$ and ignoring the high order term $O(\Delta V^2)$, we obtain:

$$L = \left[\frac{1}{s_0} + 4\alpha\sigma T_c^3 \right] \Delta V + \sigma T_c^4, \quad (3)$$

which describes a neutral state in which the dome effect is absent. Theoretically, by controlling L or T_c to obtain this special condition, one can use Eq. (3) to find s_0 .

For commercial Eppley PIRs, instead of Eq. (2), a simpler formula [e.g., *Albrecht and Cox, 1974*] is usually used:

$$L = \frac{1}{s_e} \Delta V + \sigma T_c^4 + D\sigma(T_c^4 - T_d^4), \quad (4)$$

where s_e is the sensitivity of PIR provided by Eppley (Eppley does not provide D). The relation between s_e and s_0 can be obtained by equating Eq. (4) and Eq. (2a), and ignoring $O(\Delta V^2)$:

$$\frac{1}{s_e} = \frac{1}{s_0} + 4\alpha(1+D)\sigma T_c^3. \quad (5)$$

For example, if $T_c = 300$ K, $s_e = 4 \mu\text{V W}^{-1} \text{m}^2$, then $s_0 \approx s_e[1 + 0.017(1+D)]$. Therefore, if $D = 2$, then s_e is about 5% smaller than s_0 . Although s_e depends weakly on the case temperature, for simplicity, it is usually regarded as a constant.

The range of the dome factor can be inferred from Eq. (2c). On one hand, by weighting the transmittance curve by the Planck function at 300 K (cf. Fig. 2), we obtain the broadband mean transmittance $\tau \approx 0.34$ for a PIR (SN 32193F3). From Eqs. (2c) and (1e), this implies that $D < 2$. On the other hand, by using a very sensitive high-resolution Quantum Well Infrared Photodetector (QWIP, results presented elsewhere), we inferred that the reflection of the dome can be as high as 30%. Therefore, for $\tau = 0.34$ we get $D > 1.1$.

To find s_e and D in the laboratory, our PIRs were calibrated using a method similar to that described by *Payne and Anderson [1999]*. A blackbody cavity with temperature T_b is used as a target, which is cooled in advance and allowed to warm up gradually to room temperature. Substituting $L = \sigma T_b^4$ into Eq. (4), we have:

$$\frac{T_b^4 - T_c^4}{T_c^4 - T_d^4} = \frac{1}{s_e \sigma (T_c^4 - T_d^4)} \Delta V + D. \quad (6)$$

Thus, s_e and D can be found from linear regression by proceeding as follows. A PIR is kept at the room temperature. The dome is heated before the PIR is mounted to look into the blackbody cavity. A measurement cycle lasts about 9 minutes. Figure 3 shows calibration results for a PIR (SN 32193F3). At the beginning of a measurement cycle, the dome temperature drops rapidly. Before the dome becomes cooler than the case, the data cluster fall into the upper-right quadrant. Later, when the system approaches equilibrium, the data cluster fall into the lower-left quadrant. Applying regression to both data clusters, we obtain $s_e = 4.33 \mu\text{V W}^{-1} \text{m}^2$ and $D = 2.8$.

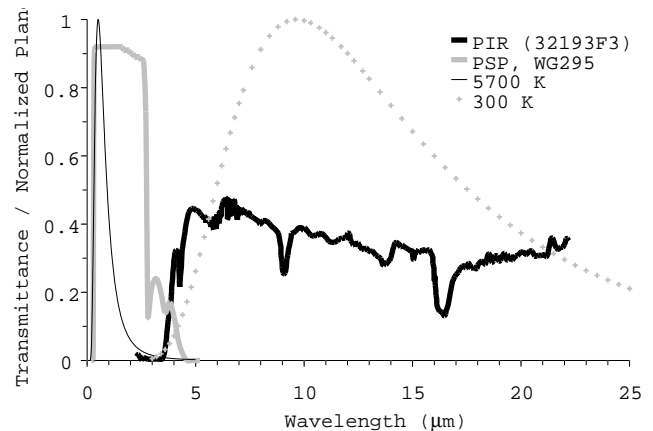


Figure 2. Transmittance of a PSP dome (Schott Glass Technologies Inc., long pass filter WG 295) and a PIR dome (silicon dome with interference filter, SN 32193F3). The normalized Planck functions at 5700 K and at 300 K are also shown.

This laboratory-determined dome factor is outside the range of $1.1 < D < 2.0$. However, if we use only the data obtained when the system approaches equilibrium (the last 6 minutes in a measurement cycle, corresponding to most of the lower-left quadrant in Fig. 3), then we get $s_e = 4.53 \mu\text{V W}^{-1} \text{ m}^2$ and $D = 1.7$. The dome factor drops into the range we expected. Note that the thermopile sensitivity is slightly higher now. For comparison, if we use only the data obtained before the system reaches equilibrium (the first 3 minutes in a measurement cycle, corresponding to all upper-right quadrant and part of the lower-left quadrant in Fig. 3), then we get $D \approx 3$.

During field campaigns, we operate two PIRs side by side. Their measurements are expected to be close to each other to within instrumental uncertainty. Using Eq. (4) and letting $L_1 = L_2$, we obtain a linear equation of the form $y = -D_1x + D_2$:

$$\begin{aligned} & \frac{(\Delta V_1/s_{e1} + \sigma T_{c1}^4) - (\Delta V_2/s_{e2} + \sigma T_{c2}^4)}{\sigma(T_{c2}^4 - T_{d2}^4)} \\ &= -D_1 \frac{T_{c1}^4 - T_{d1}^4}{T_{c2}^4 - T_{d2}^4} + D_2. \end{aligned} \quad (7)$$

Ideally, by using this equation, the measurements of the two PIRs will fall into a straight line, where the intercept (D_2) and the negative value of the slope (D_1) are the dome factors for the two instruments. When we have the PIR sensitivities, we can use Eq. (7) to derive the dome factors from field measurements. Figure 4 shows results analyzed during the Aerosol Recirculation and Rainfall Experiment (Skukuza, South Africa, August 1999). We used 4,318 pairs of one-minute data, averaged every 10 minutes. The thermopile sensitivities are derived from the laboratory calibration data for the two PIRs (SN 32193F3 and SN 32194F3) obtained during the equilibrium phase of the calibration cycle. The linear regression reveals that $D_1 = 1.7$, $D_2 = 1.6$. Again, using 16,277 pairs of nighttime data from the Dust Experiment to Study IR Extinction (China Lake, CA, November 1999), we get $D_1 = 1.6$ and $D_2 = 1.8$. These results agree well with those derived from laboratory calibrations. This implies that the nighttime measurements achieve an equilibrium state. In con-

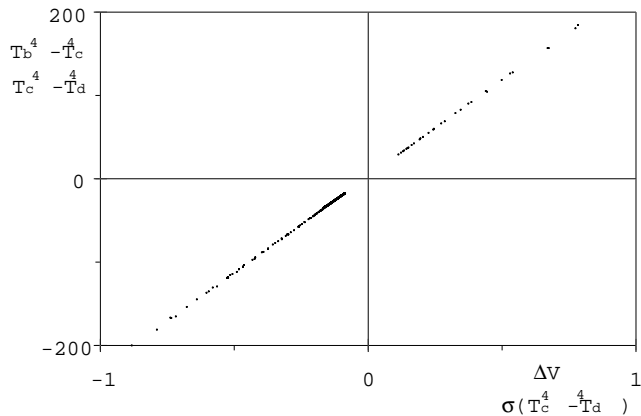


Figure 3. Calibration data for PIR (32193F3) plotted according to Eq. (6). Among the 734 data points, 29 of them fall in the upper-right quadrant where $\Delta V/(\sigma(T_c^4 - T_d^4)) > 0$ because the dome is warmer than the case.

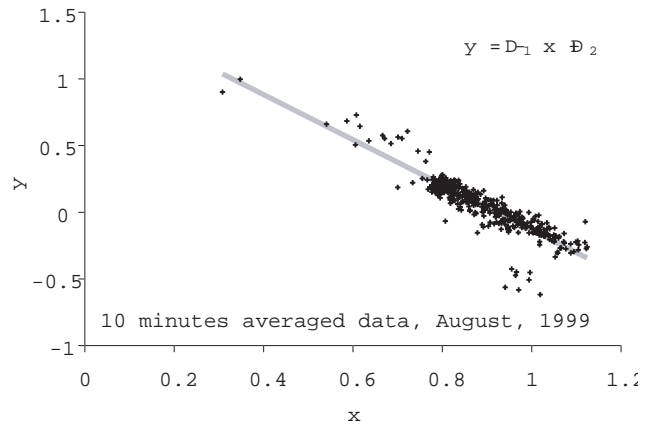


Figure 4. Nighttime field measurements of two PIRs plotted by using Eq. (7). Linear relationship between x and y is expected for an equilibrium system.

trast, the daytime data do not show such a good linear relationship between x and y in Eq. (7), implying additional non-equilibrium effects. Furthermore, if the dome factors derived by using Eq. (7) do not agree with those derived from laboratory calibrations, then it may indicate some inconsistencies in the measurements.

Finally, by using a larger dome factor, $D = 2.8$ and $s_e = 4.33 \mu\text{V W}^{-1} \text{ m}^2$, instead of using $D = 1.7$ and $s_e = 4.53 \mu\text{V W}^{-1} \text{ m}^2$, we get a larger dome effect term in Eq. (4), and lower irradiance values. The discrepancy can reach 3%, or about 10 W m^{-2} around noon during clear days. Under cloudy conditions, during nighttime, or if a PIR is shaded, the discrepancies would be smaller.

4. PSP Thermal Dome Effect

Similar to section 3, but by solving Eq. (1) for shortwave irradiance S ($\tau_{\text{sw}} \approx 1$), we get

$$S = \left(\frac{1 - \rho_d}{\epsilon_s} + \rho_d \right) k \alpha \Delta V + \epsilon_d (\sigma T_s^4 - \sigma T_d^4) + \tau (\sigma T_s^4 - L). \quad (8)$$

The first term on the right hand side is the output of a PSP. The remaining terms are usually not measured, therefore, ignored. They are commonly referred as dark-offset, zero-offset, or something similar [e.g., *Gulbrandsen, 1978*]. Now we can consider the second term as the thermal dome effect of a PSP, and the third term as the influence of the ambient longwave radiation (“longwave leak”).

Bush et al. [2000] added thermistors to a PSP and tested it in a dark room under different ambient conditions. They found an “offset” ΔF (W m^{-2}), and they propose to utilize the following empirical correction for the “systematic offset error” in PSP instruments:

$$\Delta F = a(T_d^4 - T_s^4) - b. \quad (9)$$

For their PSP dome, they derived $a = 4.0537 \times 10^{-8}$, and $b = 0.0828$.

Comparing Eq. (8) to Eq. (9), we get $a = -\epsilon_d \sigma$ and $b = -\tau (\sigma T_s^4 - L)$. b is not a constant. However, for a PSP dome, the longwave transmittance τ is small (cf. Fig. 2), so b is small. Also, if the sensor reaches thermal equilibrium with the longwave environment (i.e., $\sigma T_s^4 = L$), then $b = 0$. Using the QWIP, we find that a PSP dome is thermally

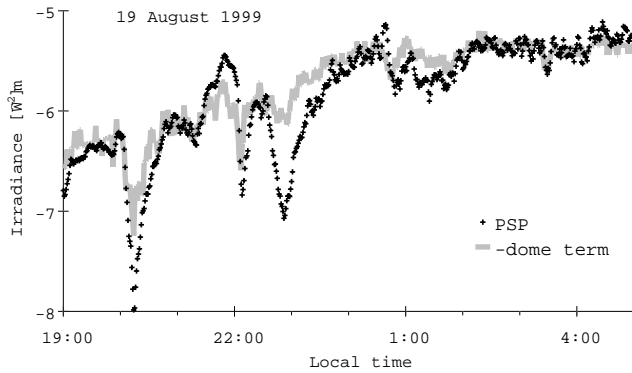


Figure 5. Nighttime measurements of a PSP (32188F3) comparing to the calculated values based on the thermal dome effect term in Eq. (8).

opaque with some reflection. If $a = 4.0537 \times 10^{-8}$, then $\epsilon_d = 0.71$. This implies that the thermal reflection of a PSP dome is about 29%.

During nighttime $S = 0$ in Eq. (8), therefore, the PSP thermopile outputs are approximately equal to the negative values of PSP thermal dome effect term. An example is shown in Fig. 5, where we approximate $\epsilon_d = 0.71$, $(T_c)_{\text{PSP}} = (T_c)_{\text{PIR}}$, and $(T_d)_{\text{PSP}} = 0.996(T_d)_{\text{PIR}}$, using collocated PIR/PSP measurements and Eq. (1f) for T_s . Figure 5 demonstrates that the thermal dome effect causes the nighttime PSP negative outputs. During daytime, solar heating and other effects on PSP are involved. Therefore, to better calibrate PSPs and to calculate the dome effect, the case and the dome temperatures of the PSP should be measured. Nonetheless, as a speculation, if we simply extend the nighttime approximation into the daytime, then there would be over 3% underestimation in PSP measurements, or up to about 25 W m^{-2} at noon.

5. Conclusion

The theory illustrated in Fig. 1 is highly simplified. However, it appropriately explains the PIR dome effect and the PSP thermal dome effect. For PIRs, we showed that when PIRs approach equilibrium with a blackbody target during calibration, the inferred dome factor becomes smaller. For our two PIRs, the dome factors are about 1.7 for equilibrium conditions, but close to 3 otherwise. For PSPs, we derived an energy balance equation, which confirms the measurement results of *Bush et al.* [2000]. We provided an example indicating that the thermal dome effect causes larger than 5 W m^{-2} PSP nighttime negative outputs. The daytime PSP thermal dome effect is more complex. To properly account

for the effect, it is essential to measure the case and the dome temperatures.

Acknowledgments. This research is supported by NASA's Radiation Science Program, managed by Dr. Robert J. Curran. Field campaigns were also supported by ONR's Marine Meteorology Program, managed by Dr. Ronald J. Ferek. Special thanks are due to Dr. Ellsworth G. Dutton and his group at NOAA Climate Monitoring and Diagnostics Laboratory for calibrating our pyrgeometers and for valuable discussions.

References

- Albrecht, B. A., and S. K. Cox, Pyrgeometer measurements from aircraft, *Rev. Sci. Instrum.*, *45*, 33-38, 1974.
- Bush, Brett C., Francisco P. J. Valero, A. Sabrina Simpson, and Lionel Bignone, Characterization of thermal effects in pyranometers: a data correction algorithm for improved measurement of surface insulation, to appear in the *J. Atmos. Oceanic Technol.*, 2000.
- Charlson, R. J. and J. Heintzenberg (Eds.), *Aerosol Forcing of Climate*, 432 pp, John Wiley & Sons, New York, 1995.
- Fairall, C. W., P. O. G. Persson, E. F. Bradley, R. E. Payne, and S. P. Anderson, A new look at calibration and use of Eppley Precision Infrared Radiometers. Part I: theory and application, *J. Atmos. Oceanic Technol.*, *15*, 1229-1242, 1998.
- Gulbrandsen, A., On the use of pyranometers in the study of spectral solar radiation and atmospheric aerosols, *J. Appl. Meteor.*, *17*, 899-904, 1978.
- Olivieri, J., Measurement of longwave downward irradiance using a PIR pyrgeometer, WMO Tech. Document, WMO/TD 453, 26 pp, 1991.
- Payne, R. E., and S. P. Anderson, A new look at calibration and use of Eppley Precision Infrared Radiometers. Part II: calibration and use of the Woods Hole Oceanographic Institution Improved Meteorology Precision Infrared Radiometer, *J. Atmos. Oceanic Technol.*, *16*, 739-751, 1999.
- Philipona, R., C. Frohlich, and C. Betz, Characterization of pyrgeometers and the accuracy of atmospheric longwave radiation measurements, *Appl. Opt.*, *34*, 1598-1605, 1995.
- Pilewskie, P., and F. P. J. Valero, Direct observations of excess solar absorption by clouds, *Science*, *267*, 1626-1629, 1995.
- Stephens, G. L., and S.-C. Tsay, On the the cloud absorption anomaly, *Q. J. R. Meteorol. Soc.*, *116*, 671-704, 1990.
- Valero, F. P. J., B. Bush, Measured and calculated clear sky solar radiative fluxes during the Subsonic Aircraft: Contrail and Cloud Effects Special Study (SUCCESS), *J. Geophys. Res.*, *104*, 27387-27398, 1999.

Q. Ji, SSAI, NASA Goddard Space Flight Center, Greenbelt, MD 20771. (e-mail: ji@climate.gsfc.nasa.gov)

S.-C. Tsay, Laboratory for Atmospheric Sciences, NASA Goddard Space Flight Center, Greenbelt, MD 20771. (e-mail: tsay@climate.gsfc.nasa.gov)

(Received September 16, 1999; revised February 2, 2000; accepted February 8, 2000.)